Design and fabrication of periodic lattice-based cellular structures

Article *in* Computer-Aided Design and Applications · August 2015

DOI: 10.1080/16864360.2015.1059194

CITATIONS
23

READS
2,123

4 authors, including:

Recep M Gorguluarslan
TOBB University of Economics and Technology
18 PUBLICATIONS **75** CITATIONS
SEE PROFILE

Umesh Gandhi
Toyota Research Institute of North America
35 PUBLICATIONS **144** CITATIONS
SEE PROFILE

Seung-Kyum Choi
Georgia Institute of Technology
62 PUBLICATIONS **925** CITATIONS
SEE PROFILE

COMPUTER-AIDED DESIGN & APPLICATIONS, 2015
http://dx.doi.org/10.1080/16864360.2015.1059194

Design and fabrication of periodic lattice-based cellular structures

Recep M. Gorguluarslan[1], Umesh N. Gandhi[1], Raghuram Mandapati[1] and Seung-Kyum Choi[2]

[1]Toyota Research Institute North America; [2]Georgia Institute of Technology

ABSTRACT

A methodology, which consists of design, optimization and evaluation of periodic lattice-based cellular structures fabricated by additive manufacturing, is presented. A user-friendly design framework for lattice cellular structures is developed by using a size optimization algorithm. A 3D modeling process for the lattice-based cellular structures is introduced for non-linear finite element analysis and production. The approach is demonstrated on compression block with periodic lattice-based unit cells. First, based on loading condition, most appropriate lattice layout is selected. Then, for the selected lattice layout, the lattice components are modeled as simple beam and size of the beam cross sections is optimized using in-house optimization approach for both yield and local buckling criteria. The 3D model for the optimized lattice structure is built and non-linear finite element study is conducted to predict the performance. Physical parts are 3D printed and tested to compare with the simulations. Material properties for the 3D printed parts are determined for the finite element study using reverse engineering of actual measured data.

KEYWORDS

Additive manufacturing; 3D Printing; lattice-based cellular structure; topology optimization

1. Introduction

The term "additive manufacturing" (AM) is applied to any manufacturing process that is used to fabricate parts directly from 3D CAD models by adding material in layers. AM technique, commonly known as 3D printing technique, offers great possibilities for fabricating parts with high complexity and customizability such as cellular structures which are difficult, tedious and time consuming, if not impossible, to produce using conventional manufacturing processes [8].

The concept of the cellular structures, including foams, honeycombs, lattices, and similar constructions, comes from keeping material only in the vital regions of a part to attain a lightweight structure while maintaining the high specific mechanical properties such as strength and energy absorption. Lattice-based cellular structures offer inherent advantages over foams due to their ability to provide light-weight and stronger materials [6], [20]. Ashby chart [2] in Fig. 1 illustrates that lattice structures can fill the gap that is needed for lightweight applications.

Although lattice structures provide high strength-to-weight ratio, the traditional CAD modeling design optimization techniques are not sufficient for design of lattice-based cellular applications due to their geometry complexity. In order to effectively design cellular structures, the material properties must be characterized and the structures should be carefully modeled. Then, their performance must be quantified, as well. Many studies have been conducted addressing such challenges in the last two decades [17], [19]. Johnston et al. [10] has provided a comprehensive analytical model by considering each member in the octet lattice structure as a beam element and showed that finite element (FE) modeling of the lattice structures is relatively easier when beam elements are used. Ruderman et al. [16] and Patel and Choi [14] have introduced a topology optimization methodology to determine the optimized cross-sectional parameters of lattice based unit cell of a pressure tank utilizing beam elements in FE modeling with linear material properties. Although using beam elements facilitates the modeling and optimization of lattice-based structures, beam elements cannot represent the 3D geometry of the structure. Therefore, lattice-based structures modeled using beam elements cannot be fabricated using AM techniques. In addition, the non-linearity of the material and geometry of lattice-based structures has to be considered in finite element analysis (FEA) for accurate results compared to the physical experiments under large deformations.

In order to overcome the aforementioned issues, a methodology for design and fabrication of lattice-based cellular structures is introduced in this study. Specifically, FE software Abaqus is employed for FE modeling and

CONTACT Recep Gorguluarslan rmg@gatech.edu

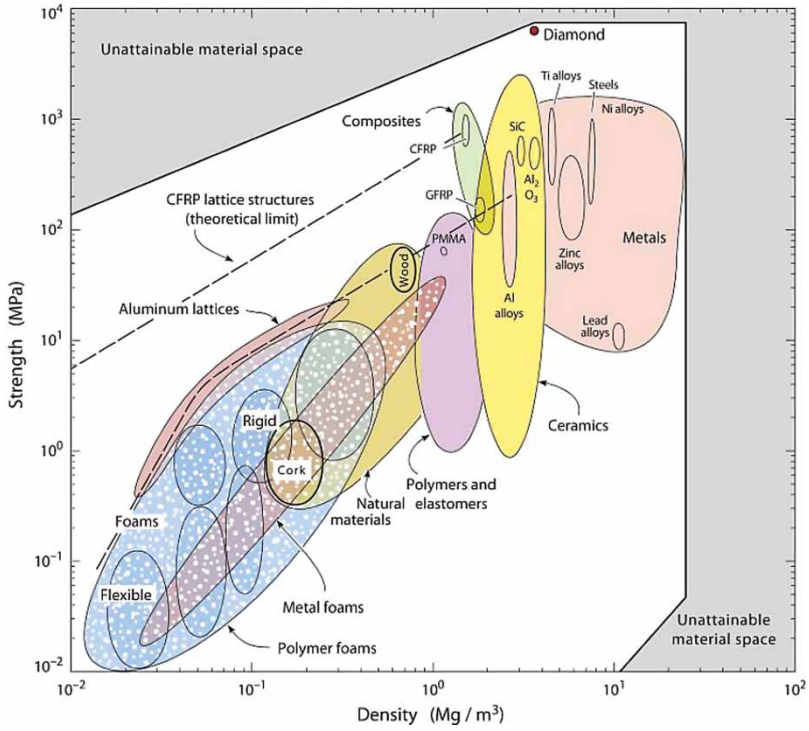

Figure 1. Strength vs. Density chart for engineering materials. There is a gap in the low density high strength region which could be filled by lattice structures.

analysis of lattice-based cellular structures in the optimization process. The 3D geometry of the optimized lattice structures is created using 3D printing software Netfabb [12]. The geometry is generated in STL format since it is the required format for 3D printing. The 3D geometry generated is also converted to a solid geometry with brick elements using commercial FE modeling tool Hypermesh [9] in order to conduct the non-linear FEA with non-linear material properties. The approach is demonstrated on a compression block with periodic lattice-based unit cells. First, most appropriate lattice layout is selected based on the loading condition. Then, for the selected lattice layout, the lattice components are modeled as simple beam and size of the beam cross sections are optimized using the in-house optimization approach. Finally, the 3D model for the compression block is built using the optimized lattice structure and non-linear FE study is conducted to predict the performance. Physical parts are also build using 3D printers and tested to compare with the simulations. The compression block design is optimized for both yield and local buckling criteria. In order to achieve the realistic design of the block, the material properties for the 3D printed parts were determined for the FE study using reverse engineering of actual measured data.

The paper is organized as follows. Section 2 introduces the optimization procedure used for the lattice structure with two different formulations by considering failure due to yield and buckling. Section 3 describes the design procedure of the lattice-based cellular structures from optimization to 3D geometry generation and fabrication. In Section 4, a lattice-based compression block design utilizing the introduced design procedure is presented and non-linear simulation results are validated by physical experiments.

2. Optimization of lattice-based cellular structures

The extension of design optimization to the optimization of material layouts is known as topology optimization. Topology optimization operates on a fixed FE mesh of either continuum or discrete elements to optimally distribute material in the material layout [4]. For continuum structures the shape of the external and internal boundaries and the number of holes are optimized [3]; whereas, for the discrete structures, the topology problem is solved by determining the optimum number, the position, and the mutual connectivity of structural member elements [15]. In discrete or ground truss approach, a ground structure, which is a grid of all elements connecting the nodes in the design space, is optimized selecting optimal cross section parameters of the ground truss members. In other words, each element is associated with a design variable that defines the element size or its contribution to the entire topology [14]. The converged optimization

result is supposed to drive the value of all the design variables either close to the lower and upper limits so that a definite topology is defined. The main objective is to achieve the objective function with the minimum amount of material as possible. The formulation of a ground-truss optimization is given by

$$\textit{Find} \quad b \tag{2.1}$$

$$\textit{Min} \quad f(b) \tag{2.2}$$

$$\textit{subject to} \quad g_j(b) - g_{j,allow} \leq 0 \tag{2.3}$$

$$\sum_{i=1}^{N} A_i L_i - V_{allow} \leq 0 \tag{2.4}$$

$$b_l \leq b \leq b_u \tag{2.5}$$

where $f(.)$ represents the objective function and b denotes the vector of design variables (i.e. cross-sectional parameters) in Eq. (2.1) and (2.2). The function, g_j, denotes the additional constraints such as stress and $g_{j,allow}$, denotes the allowable value for this function in Eq.(2.3). A_i is the cross-sectional area of the elements and L_i is the length of that particular element in Eq. (2.4). V_{allow} denotes the maximum allowable volume of the material that can be used in the final design. The upper and lower bounds of design variables are denoted by b_u and b_l in Eq. 2.5., respectively.

Ultimately, the ground-truss approach is a sizing optimization problem, where the cross-sectional parameters of lattice members are the continuous design variables. The cross-sections of the members are sized to support the applied loads on the structure. The members with cross-sections near zero are then removed to obtain the optimal structure. In the optimization process, FEA is invoked and the information required by the objective function is evaluated at each iteration. The steps of the optimization process are given as follows:

1. Initial feasible finite element model (FEM) is generated using the inputs such as geometry, loading and boundary conditions. The cross-sectional parameters (e.g. thickness, radius, etc.) are the design variables in the optimization process.
2. FEA of the generated model is carried out using an FE solver.
3. The optimization formulation given by Eqs. (2.1) - (2.5) is evaluated by the optimization algorithm and the improved design is obtained.
4. If the results of FEA satisfy the objective and constraints in the optimization formulation and converge, then the optimization stops and the optimal design is determined.
5. Otherwise, the design variables are updated and Steps 2–4 are repeated.

The flowchart of the optimization procedure of lattice structures is illustrated in Fig. 2.

2.1. *Stress-based optimization of lattice-based cellular structures*

For the optimization with beam elements, the failure due to yield is not seen in the FEA of the structure since only linear material properties are used. Hence, the stress constraint has to be included into the optimization procedure. In addition, we expect the lattice structure to withstand the applied loads with minimum deflection. Hence, the objective is to minimize the maximum displacement in the structure. The optimization formulation (i.e. Eqs. (2.1)-(2.5)) is modified based on these criteria. Circular cross-sections are used in this study and therefore the design variables are the radius values of the elements in the lattice structure. Thus, the stress-based optimization procedure minimizes the maximum displacement (d_{max}) to determine the optimal radii of the members in the unit cells (r_i) such that the maximum von Mises stress in

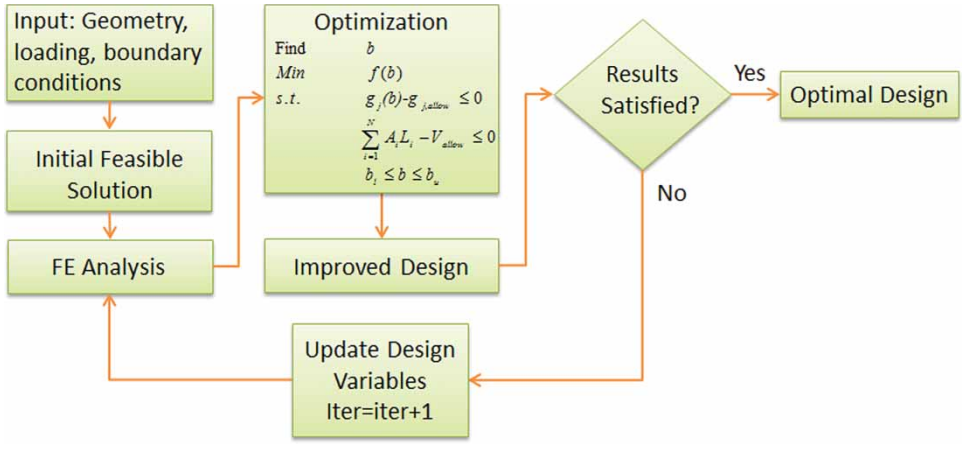

Figure 2. Flowchart of the lattice structure optimization process.

the structure (S_{max}) will be less than the allowable stress (S_{allow}):

$$\begin{aligned} &\textit{Find} && r_i;\ i = 1, \ldots, N && (2.6)\\ &\textit{Minimize} && d_{\max} && (2.7)\\ &\textit{Subject to} && V_{total} - V_{\max} \cdot Vol\_Frac \leq 0 && (2.8)\\ & && S_{\max} - S_{allow} \leq 0 && (2.9)\\ & && r_{lb} \leq r_i \leq r_{ub} && (2.10) \end{aligned}$$

where r_{lb} and r_{ub} are the lower and upper bounds of the design variables r_i. The final volume of the structure (V_{total}) must be less than or equal to a fraction (Vol_Frac) of the maximum volume (V_{max}) which is the volume of the structure when all radii are equivalent to r_{ub}. The volume of the optimized structure (V_{total}) and the maximum volume (V_{max}) with circular cross sections are calculated by

$$V = \sum_{i=1}^{n} \pi \cdot r_i \cdot L_i \tag{2.11}$$

where n is the number of members in the structure and L_{i} are the length of each element.

2.2. *Buckling-based optimization of lattice-based cellular structures*

Linear buckling is one of the failure mechanisms for the lattice structures under compression. Buckling is defined as the deformation at which the lattice structure exhibited a visibly large transverse deformation and a rapid decrease of the resistance to deformation was observed [18]. Failure due to buckling can occur before yield strength on the elastic region especially for thin wall structures under compression. Therefore, buckling has to be taken into account for the optimization of the lattice-based cellular structures.

The critical load that causes buckling on the lattice structure can be determined by eigenvalue linear buckling analysis method. The eigenvalue that is found with the analysis is the linear prediction of the buckling load. The linear eigenvalue problem is given by

$$(K_0^{NM} + \lambda_i K_\Delta^{NM})\ v_i^M = 0 \tag{2.12}$$

where $K_0{}^{\text{NM}}$ is the stiffness matrix to the base state including the effect of the preloads (P^N), $K_\Delta{}^{\text{NM}}$ is the differential initial stress and load stiffness matrix due to the incremental loading pattern Q^N, λ_{i} are the eigenvalues, $v_{\text{i}}{}^{\text{M}}$ are the buckling mode shapes, M and N are the degrees of freedom for the whole model and i refers to the i^{th} buckling mode. Then, the critical buckling load becomes [1].

$$F_b = P^N + \lambda_i Q^N \tag{2.13}$$

The buckling loads are calculated relative to the base state of the structure. The preload P^N is often zero for classical eigenvalue problems. When a structure is loaded by a compressive unit force, the resulting first eigenvalue, λ_1, represents the critical buckling load, F_{b}

In buckling-based optimization of the lattice structures with the proposed procedure the objective is to maximize critical load obtained by the eigenvalue buckling analysis such that the volume of the structure (V_{total}) will be less than or equal to the pre-determined allowable volume (V_{allow}). Thus, the optimal cross-sectional parameters (i.e. radii, r_{i}) of members in the lattice structure, which satisfy this objective and constraint under a unit compression load, are determined. The optimization formulation, given by Eqs. (2.1) – (2.5), is modified for buckling-based optimization as follows:

$$\begin{aligned} &\textit{Find} && r_i;\ i = 1, \ldots, N && (2.14)\\ &\textit{Maximize} && F_b && (2.15)\\ &\textit{Subject to} && V_{total} - V_{allow} \leq 0 && (2.16)\\ & && r_{lb} \leq r_i \leq r_{ub} && (2.17) \end{aligned}$$

3. Design and modeling methodology for lattice-based cellular structures

Computer technologies such as CAD and CAE are widely used for the design of engineering parts and systems. As mentioned earlier, due to the geometric complexity of the lattice structures, it is impractical to use the existing CAD modeling techniques for lattice-based applications. The lattice geometry can easily be modeled using linear beam elements for the purpose of FEA of these structures as but beam elements cannot accurately take the non-linear geometry deformation and/or non-linear material behavior into account. The 3D solid model of the lattice structures is necessary to be built using brick elements for non-linear FEA. In addition, beam elements cannot represent the 3D geometry of the lattice structures which is required for 3D printing of the structures. Hence, advanced modeling techniques are required to investigate the non-linear behavior of a lattice structure by FEA and to fabricate the designed structures. In this study, a design methodology that can overcome all of the issues mentioned above is developed and applied for the design of a lattice-based compression block. The proposed design procedure is illustrated in Fig. 3.

The first step of the design procedure is to choose the most efficient lattice layout. For this purpose, the structure is modeled using different lattice types and FE

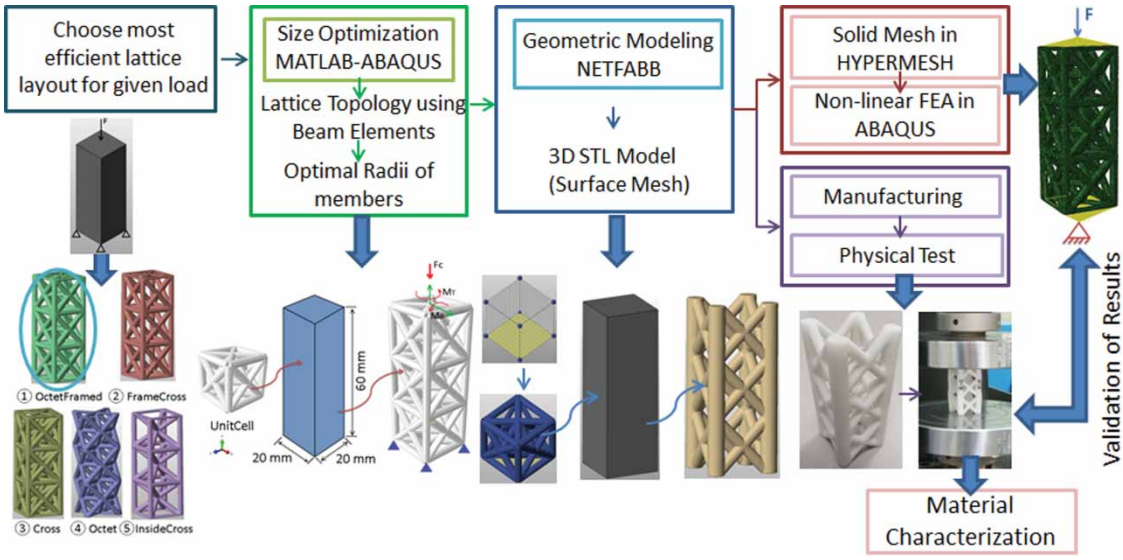

Figure 3. Proposed design procedure of lattice-based cellular structures.

simulations are conducted in defined loading and boundary conditions to evaluate their performances. The lattice type, which gives the highest performance, is used in the optimization procedure given in Section 2. After the topology and optimal cross-sectional parameters of the lattice members are determined, the 3D geometry of the structure has to be created for nonlinear FEA and manufacturing of the physical part. Commercial 3D printing software Netfabb is used for creating the 3D geometry of lattice based structures in the proposed procedure. It enables 3D modeling of complex lattice structures easily and allows exporting the geometry as an STL model.

For non-linear FEA, 3D solid model of the structure is required. For this purpose, the STL model, which contains triangular surface meshes as the definition of the geometry, has to be converted into the FEM with the solid/brick elements. This conversion can be achieved by commercial FE modeling tool HyperMesh. Existing surface mesh information in the STL file is used to create the solid model of the structure with tetragonal 3D elements using this tool. This FEM of the lattice structure with 3D solid elements is then used in Abaqus in order to perform non-linear FEA with non-linear material properties.

Since 3D STL model is the required format for 3D printing, these models created in Netfabb can be used for the manufacturing of the structures using 3D Printing machines. Then, the produced parts can be physically tested for the validation of the non-linear FEA results. In addition, the material properties used in FEA can be determined by the test results. The design procedure shown in Fig. 3 is implemented for lattice-based compression block design in the following section.

4. Design of lattice-based compression block

The proposed design and modeling procedure explained in Section 3 is implemented to the design, modeling, production and validation of a $20 \times 20 \times 60$ mm compression block with lattice cell structures shown in Fig. 3. Before the design procedure, two different materials produced by two different additive manufacturing methods are investigated to determine the strongest material for the design. Non-linear material properties, which will be used in the FEA of the structures, are determined for these materials using reverse engineering. The one with better mechanical properties is chosen for the design of the lattice based compression block. Then, the compression block is modeled with various lattice types and the one with the highest performance is chosen for the size optimization. The lattice-based compression block is optimized using both stress-based and buckling-based optimization procedures explained in Section 2. The 3D solid models of the optimized parts are created and non-linear FEA is performed. FEA results of the optimized parts are validated by the experimental results.

4.1. *Material characterization and selection for the lattice-based compression block design*

The published material properties of the materials used in 3D printing may not be accurate due to the inherent layer by layer manufacturing process of the 3D printing machines. Hence, first, the material properties have to be determined by experiments using the 3D printed structures. The mechanical properties of two different materials; Nylon 6 used with Selective Laser Sintering

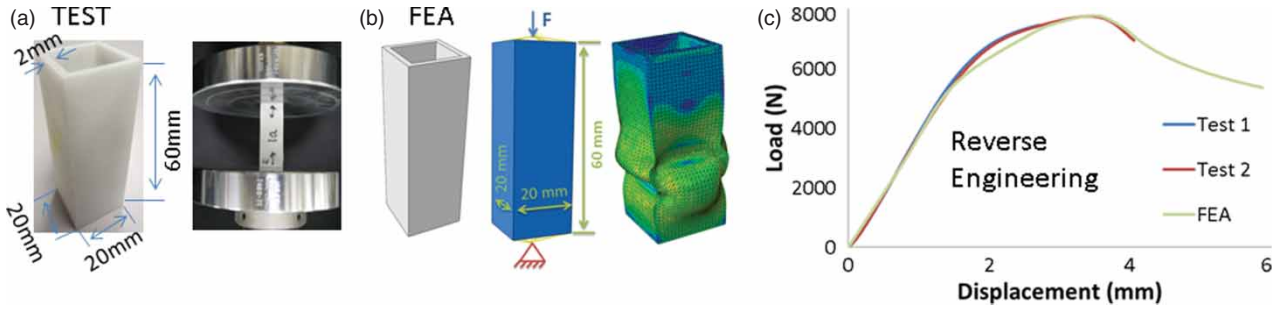

Figure 4. (a) Produced hollow box and physical compression test, (b) FEA of the hollow box, (c) Load vs. Displacement curves obtained by tests and FEA.

(SLS) and Nylon 12 used with Fused Deposition Modeling (FDM) technique; are estimated and compared in this section. Since the purpose was merely the characterization of the materials, these AM processes are not explained in detail. One can refer to Ref. [8] for detailed descriptions of both AM techniques.

4.1.1. *Material properties of Nylon 6*

For the estimation of the material properties of Nylon 6 material, a hollow box with 2 mm thickness, shown in Fig. 4(a), is modeled, produced by SLS technique and physically tested under compression. The load vs extension curve obtained by the compression test is converted to stress-strain curve to estimate the Young's modulus and elastic-plastic material curve of the material. The stress values can be simply obtained by dividing the force by the area of the cross section. The strain is calculated by dividing the displacement by the length of the structure. The Young's modulus is calculated by the linear portion of the stress-strain curve while the plastic material properties are obtained with the non-linear portion of the curve. Then, the non-linear FEA of the hollow box is conducted using the determined material properties of Nylon 6 (Fig. 4(b)). The FEA results and experimental results are compared in Fig. 4(c). The estimated elasticity and yield strength values are found to be less than the published bulk material properties as given in Table 1.

Table 1. Material properties of NYLON 6.

Properties	Young's Modulus	Yield Strength
Published Data [13]	1,600 MPa	46 MPa
Reverse Engineering	1,478 MPa	36 MPa

4.1.2. *Material properties of Nylon 12*

For the estimation of the material properties of Nylon 12 material, tensile test coupons are built in three different directions in FDM process as shown in Fig. 5(a) to investigate the material properties in each direction. The tensile tests are conducted (Fig. 5(b)) to obtain tensile load vs. displacement curves of the coupons. The test results in Fig. 5(c) show that the parts produced along X and Y axes have similar curves while there is a 10% difference for the parts produced along Z axis. This difference is not so distinctive and therefore it is assumed that the material is isotropic for determining the material properties.

The data of the sample produced along Y axis is converted to stress-strain curve to estimate the elasticity modulus and elastic-plastic material curve. The Young's modulus is determined by the linear portion of the stress-strain curve. The plastic strain data is obtained by the rest of the data by the true stress-strain calculation. Fig. 5(c) shows that the experimental and FEA results match well along Y and X axis but different from the ones produced

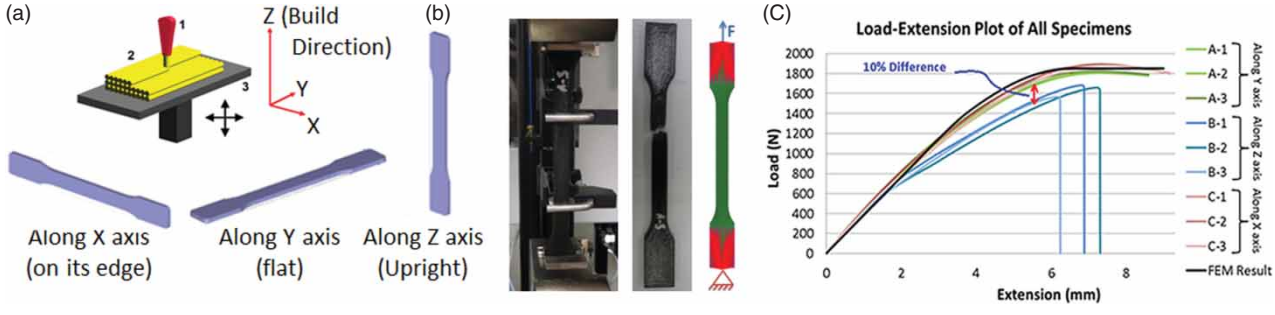

Figure 5. (a) Building directions in FDM process, (b) Tensile test and FEA model (c) Load vs. Displacement curves of tensile tests and FEA.

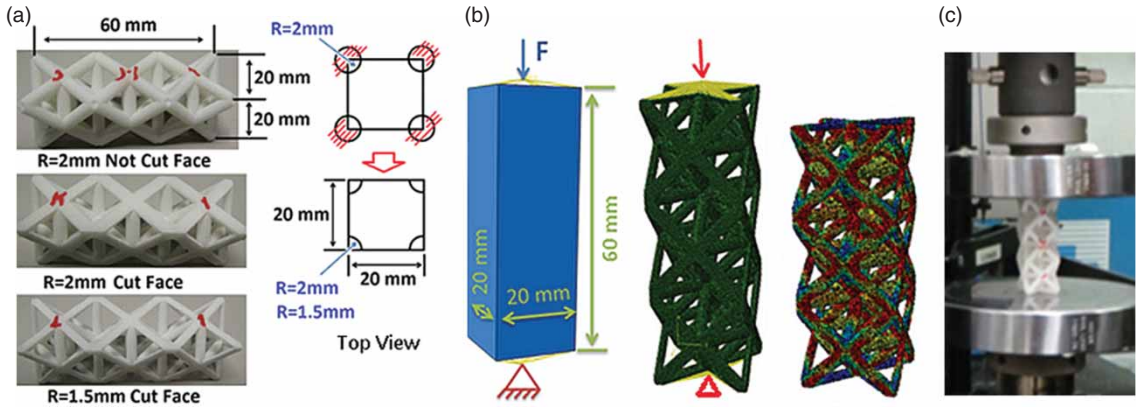

Figure 6. (a) Models of the compression block with periodic octet cell (b) Dimensions of compression block modeled with octet cell and FEM of lattice structures, (c) Physical compression test.

along Z axis since the material properties are estimated using the data of the part produced along Y axis.

The estimated elasticity and yield strength values are found to be less than the published bulk material properties as given in Table 2.

Table 2. Material properties of NYLON 12.

Properties	Young's Modulus	Yield Strength
Published Data [7]	1310 MPa	44 MPa
Reverse Engineering	1,030 MPa	30 MPa

4.1.3. *Comparison of mechanical performance for Nylon 6 and Nylon 12*

The mechanical performances of these two materials are compared for a $20 \times 20 \times 60$ mm compression block modeled with periodic octet unit-cell with $20 \times 20 \times 20$ mm dimensions in three different cross sectional sizes: One with 2 mm radius for each strut member; one with 2 mm radius and cut faces on the surfaces; and one with 1.5 mm with cut faces on the surfaces (Fig. 6(a)). The modeling procedure explained in Section 3 is used for FE modeling with 3D solid mesh and non-linear FEA (Fig. 6(b)). The models are loaded with an applied displacement perpendicular to the top surface, while the base of the model was constrained in the loading direction. This combination of applied displacement and constraints simulates the conditions of the mechanical characterization, with the only notable difference being the friction between the sample and the patterns in the mechanical tests. The total reaction force of all nodes from the bottom surface was computed. The purpose of the numerical modeling was to show that numerical methods can be used to predict the compression behavior of complex lattice structures; hence it is possible to use these methods to optimize cellular structures for any given application.

The lattice structures are also built by SLS and FDM processes with corresponding materials and the compression tests are conducted at for two different materials (Fig. 6(c)). The load vs displacement results of the tests

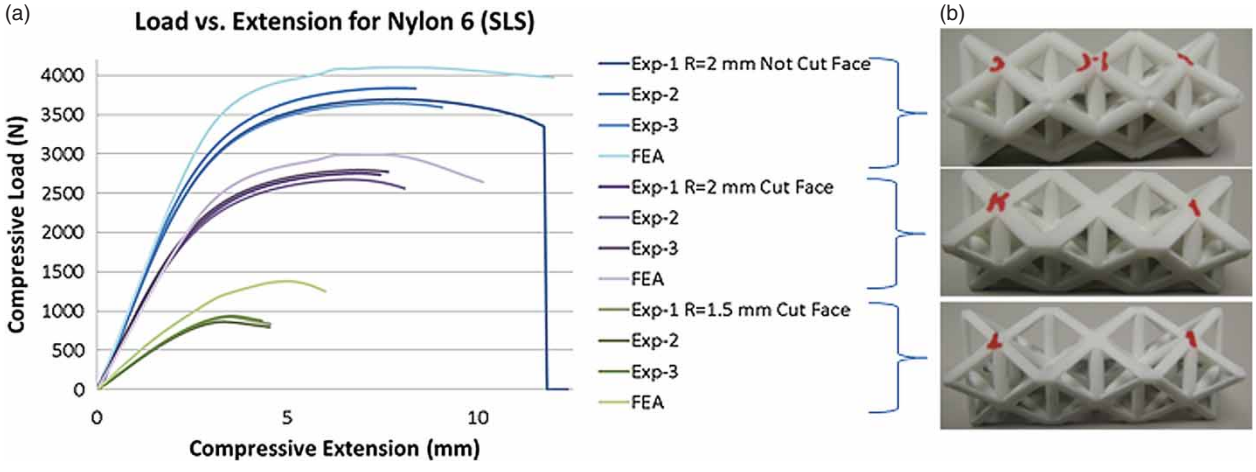

Figure 7. (a) Load vs Deformation curves for structures with Nylon 6 (b) Produced structures by SLS.

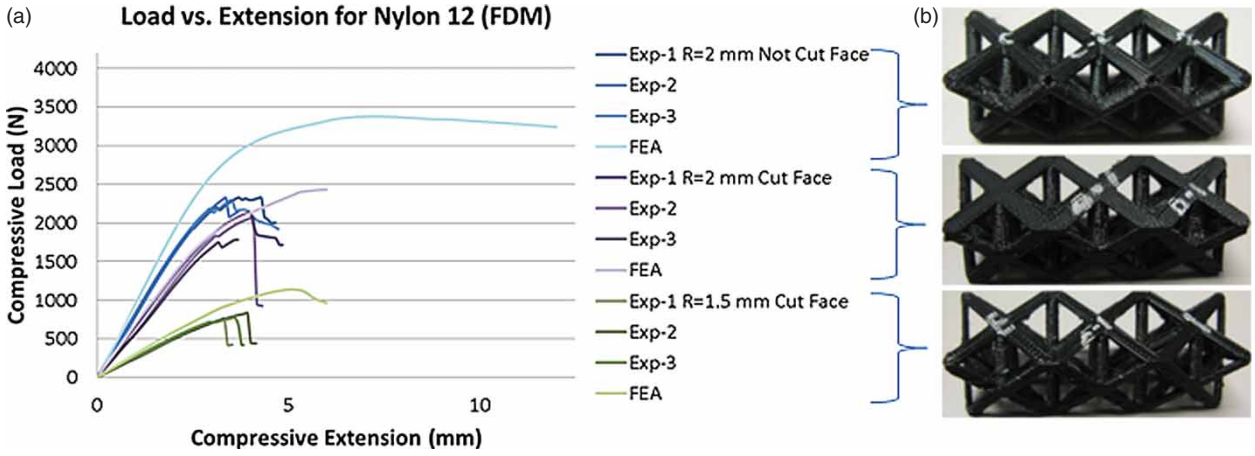

Figure 8. (a) Load vs Deformation curves for structures with Nylon 12 (b) Produced structures by FDM.

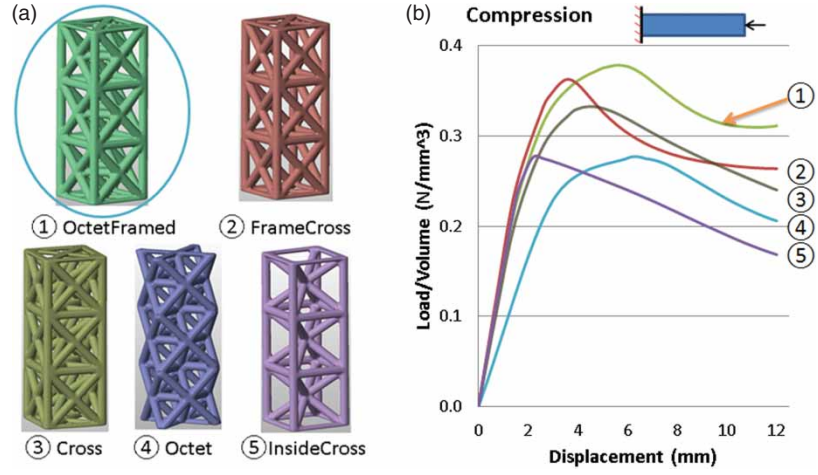

Figure 9. (a) 5 different lattice types, (b) Non-linear FEA results in compression.

are compared with FEA results in Fig. 7 for Nylon 6 and in Fig. 8 for Nylon 12.

As can be seen in Fig. 7 and Fig. 8, the isotropic material properties predicted for both materials provide FEA results that show good agreement with the test results. Due to the differences in building directions with FDM process, the parts produced by Nylon 12 material failed earlier than the FEA results as seen in Fig. 8. On the other hand, for the parts build by SLS process, even the nonlinear portion of the curves obtained by FEA with isotropic material properties agree well with the experimental results as seen in Fig. 7. Hence, the isotropic material properties that were predicted in the previous section can be used for the simulations of the lattice structures. In addition, it is observed that the parts produced by SLS with Nylon 6 material take higher compressive loads than the ones built by FDM with Nylon 12 material. From the test results, the largest load on the parts produced by Nylon 6 is about 3800N while it is 2400N for Nylon 12. Since Nylon 6 has higher strength at the same compression displacement than Nylon 12it can be chosen as the material that is used in the optimization process of lattice based compression block.

4.2. *Lattice type selection*

For the purpose of determining the best lattice layout, the compression block with $20 \times 20 \times 60$ mm dimensions is modeled with five different unit cell types as shown in Fig. 9(a). Each unit cell in the periodic lattice structures has $20 \times 20 \times 20$ mm dimensions with 1.5 mm radius for each member in the cells. 3D solid FE models of the structures are prepared and simulated via non-linear FEA the estimated non-linear material properties of Nylon 6 to explore the performance of the structures in compression. Since the volume of the structure changes with the type of lattice structure the load per volume vs displacement results are shown in Figure 9(b) for a better comparison. It is seen that OctetFramed structure has the highest load carrying capacity in compression. Hence,

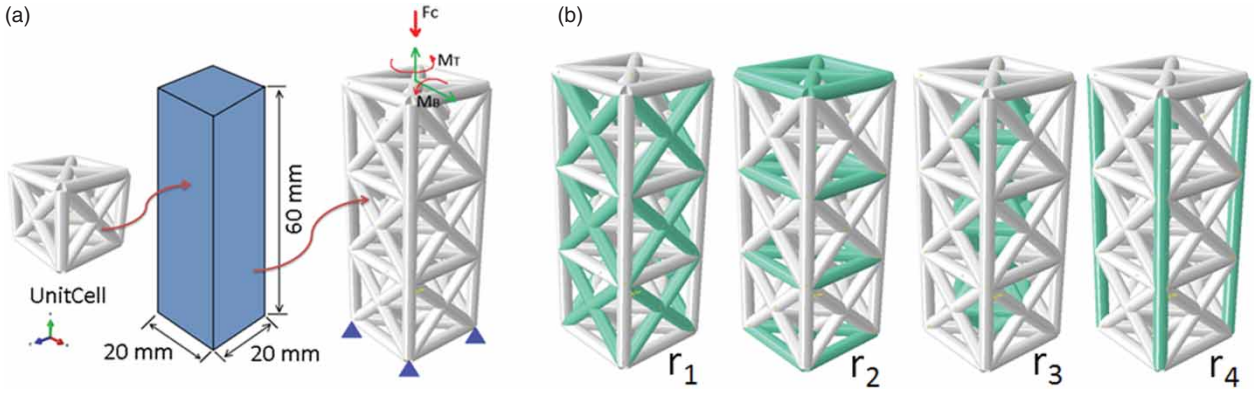

Figure 10. (a) FE modeling of compression block with OctetFramed lattice type using beam elements. (b) Four design variables r_1-r_4 determined in the optimization procedure.

Octet Framed is used in the optimization procedure as the lattice type to be optimized.

4.3. *Stress-based optimization of octetframed-based compression block*

The compression block is modeled by the OctetFramed lattice type using beam elements (Fig. 10(a)) for the stress-based optimization given by Eqs. (2.6)-(2.10). There are 4 design variables determined (i.e. radii of members) as shown in Fig. 10(b), since the symmetry of the struts is used to reduce the number of design variables. The optimization is conducted under three different loading conditions as shown in Fig. 10(a); F_C represents the compression load, M_B represents the bending, and M_T represents the torsion. In addition, the combination of all three loading types is also used as the loading condition to obtain the optimum radii of the members of lattice structure.

The lower and upper bounds of the design variables required for Eq. (2.10) are determined as $r_{lb} = 0.01$ mm and $r_{ub} = 4$ mm, respectively. The maximum volume (V_{max}) required for Eq. (2.8) is calculated using Eq. (2.11) when all radii are $r_{ub} = 4$ mm. The volume fraction in Eq. (2.8) is initiated from 0.05. If there is no feasible design found, it is increased with 0.05 increments until finding a solution satisfying the constraints. The allowable stress required in Eq. (2.9) is set to the yield stress of Nylon 6 material determined by reverse engineering. 1 (i.e. $S_{allow} = 36$ MPa in Tab. 1).

Two different optimization methods are implemented:

- First, "Exhaustive search" method is utilized for the optimization. The values for each design variable is generated with 0.1 mm increment between $r_{lb} = 0.01$ mm and $r_{ub} = 4$ mm. In this method, the FE simulations are performed with each possible combination of the design variables and the results are evaluated after all simulations are done. But attempting to simulate all possible combinations requires a very high number of simulations. Hence, exhaustive search method increases the optimization time dramatically. On the other hand, it gives the global optimum since all possible combinations are evaluated.
- Since an exhaustive search is computationally too expensive, a gradient-bsed optimization method, namely "active-set" method [11] is also utilized. This algorithm enables converging to the optimal design point quickly. However, it can result in diverging from the optimal design and/or converging to local optimum design. Therefore, it may not provide the global optimum every time.

The results of the optimized structures for different loading conditions are listed in Fig. 11. It is seen that an optimal solution is obtained when *Vol_Frac* is 0.05 in compression and bending but in torsion the optimal solution exists when *Vol_Frac* is 0.1. In combined loading conditions, on the other hand, *Vol_Frac* is 0.15 in exhaustive search and it is 0.2 with the active-set method. As seen in Fig. 11, the displacement and stress values of the structures found by "Exhaustive Search" are lower than the ones found by the active-set method. As mentioned before, the reason is active-set method converges to local optimum point while exhaustive search finds the global optimum solution.

The results of the optimized structures in Fig. 11 show that the vertical frame members in the lattice structure are more important in compression and bending since the other members have very small radius values. In torsion, on the other hand, diagonal frame members are more critical. The inner diagonal members and horizontal members have the least effect on the performance. The optimized parts under the combination of compression, bending and torsion have both the vertical and diagonal frame members in exhaustive search method. While creating the 3D models of the optimized structures as shown at the bottom of Fig. 11, each member which has

	Exhaustive Search				Active-Set method			
	Comp.	Bend.	Torsion	Combin	Comp.	Bend.	Torsion	Combin
F_C (N)	1500	0	0	**1500**	1500	0	0	**1500**
M_B (N.m)	0	7500	0	**7500**	0	7500	0	**7500**
M_T (N.m)	0	0	10000	**10000**	0	0	10000	**10000**
R1	0.01	0.25	2.25	**2**	0.69	0.43	1.97	**2.3**
R2	0.01	0.25	0.01	**0.01**	0.49	0.75	0.69	**1.2**
R3	0.01	0.01	0.01	**0.01**	0.59	0.85	0.67	**0.9**
R4	2.5	2.5	0.01	**3**	1.99	1.8	0.1	**2.4**
Vol_Frac	0.05	0.05	0.1	**0.15**	0.05	0.05	0.1	**0.2**
Disp	0.78mm	1.2mm	1.24mm	**2.08mm**	1.13mm	2.26mm	1.6mm	**2.44mm**
Max_Stress	19MPa	11.7MPa	17.9MPa	**33.7MPa**	30.2MPa	30.9MPa	23MPa	**36.5MPa**

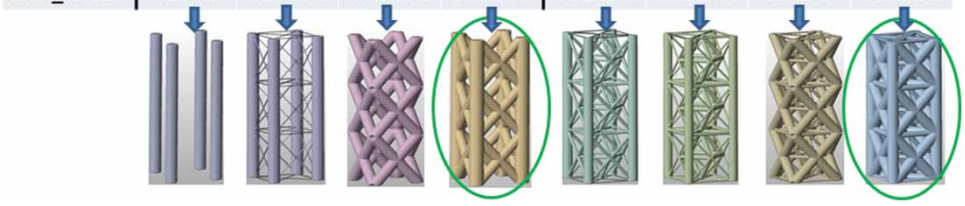

Figure 11. Optimized parts and results in different loading conditions.

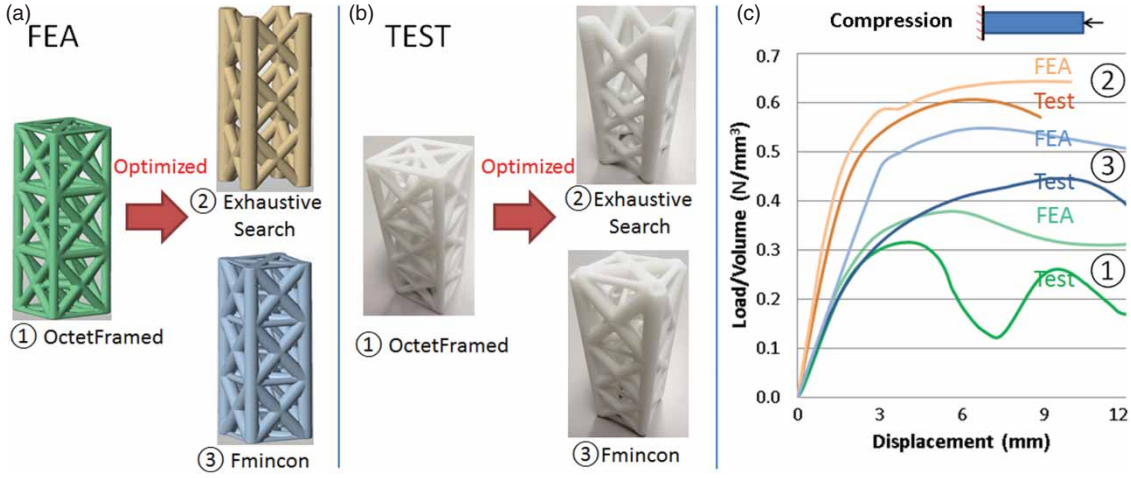

Figure 12. (a) 3D geometric models of the optimized structures (b) 3D Printed structures (c) Load per Volume vs Displacement results from FEA and compression test.

a radius equal to the lower bound (i.e. $r_{lb} = 0.01$ mm), are removed from the structure.

Although the main purpose is to improve the performance of the lattice structure under performance, we also expect it to withstand the torsional and bending moments. Therefore, the optimized structures obtained in combination of three different loading conditions, circled in Fig. 11, are our interest. In order to compare the performance of these optimized structures with the initial structure with 1.5 mm radius for each member, solid FE models of these structures are created as shown in Fig. 12(a) and non-linear FEA is carried out with non-linear material properties of Nylon 6. These structures are also built by SLS process as shown in Fig. 12(b) and the FEA results are validated with physical compression test results in Fig. 12(c).

As seen in Fig. 12(c), the optimized structures have higher load carrying capacities than the initial Octet-Framed structure with 1.5 mm radius for each member. The optimized structure with "Exhaustive Search" method has a higher load carrying capacity than the one optimized with active-set method. This validates that active-set method is trapped in local optima and therefore load carrying performance is lower. On the other hand, the optimization time with exhaustive search is about 35 hours while it is about 20 minutes with the actives-set method. Although there is a performance loss, by using an efficient optimization procedure such

as active-set method, the optimization time is greatly decreased.

4.4. *Buckling-based optimization*

When thin wall hollow structures are compressed, depending on width-to-thickness (w/t) ratio local buckling can be seen before yielding. Hence, buckling should be taken into consideration in the optimization of the lattice structures. Before the optimization of the lattice structure with buckling criteria, $20 \times 20 \times 60$ mm compression block is modeled as a hollow box with 1 mm and 2 mm thickness values in order to observe the buckling failure behavior of the structures with thin walls Eigenvalue buckling analysis in Abaqus is used to determine the critical load that causes buckling for these structures. The structures are loaded by a downward unit force as shown in Fig. 13(a).

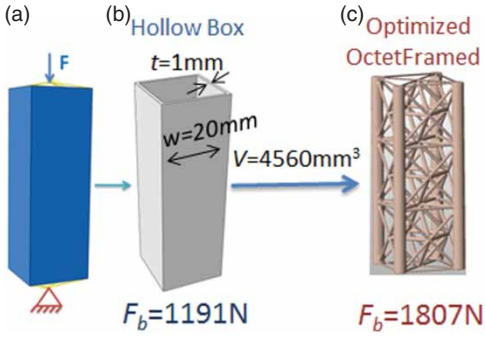

Figure 13. (a) Loading and boundary conditions for eigenvalue buckling analysis, (b) Buckling load of hollow box, (c) Buckling load of optimized OctetFramed-based structure.

The resulting first eigenvalue, obtained by the linear buckling analysis, represents the critical buckling load of the structure. In addition, the yielding load values for both hollow boxes are calculated by multiplying the yield stress of Nylon 6 material ($S_y = 36\,MPa$) by the cross-sectional areas of hollow boxes. The yielding load values and the critical buckling load values are listed in Tab. 3 for comparison.

Table 3. Comparison of buckling and yielding loads for hollow box structures.

Hollow box	Buckling Load	Yielding Load	Conclusion
t = 1 mm	1191N	2736N	Buckling before yielding
t = 2 mm	9559N	9216N	Buckling after yielding

As seen in Tab. 3, buckling occurs before yielding for the hollow box with 1 mm thickness, while yielding occurs before buckling for the hollow box with 2 mm thickness. Hence, it can be concluded that there is room to improve the buckling performance of hollow box with 1 mm thickness by using lattice-based cellular structures at the same volume. On the other hand, there is no need to consider the buckling for the hollow box with 2 mm thickness since yielding occurs prior to buckling.

Therefore, the compression block is again modeled by the OctetFramed lattice type as shown in Fig. 10(a)), using beam elements for the buckling-based optimization with Eqs. (2.14)-(2.17). Similar to the stress-based optimization, there are 4 design variables as shown in Figure 10(b), since the symmetry of the struts is used to reduce the number of design variables. For eigenvalue buckling analysis, only a unit compression load (i.e. $F = 1$N in Fig. 13(a)) is applied on the structure. In Eq. 2.16, the allowable volume (V_{allow}) is set to the volume of the hollow box with 1 mm thickness (i.e. $V_{\text{allow}} = 4560\ \text{mm}^3$) since the purpose is to improve the buckling performance of the hollow box using lattice cells. The lattice structure is optimized and the critical buckling load (F_{b}) results of hollow box and optimized OctetFramed-based structure are compared in Fig. 13(b) and Fig. 13(c), respectively. As can be seen the buckling load of the structure at the same volume is increased from 1191N to 1807N by utilizing the optimization of lattice based structures. This result proves that buckling-based optimization can improve the performance of the structure when buckling occurs prior to yielding.

4.5. *Energy absorption of optimized structures*

In previous section, it is shown that yielding is the first criteria for 2 mm hollow box. Hence, its performance is compared with the performances of the structures obtained by stress-based optimization shown in Fig. 14(a). For this purpose, the non-linear FEA of initial OctetFramed-based structure, the optimized structures with stress-based optimization given in Fig. 12(a) and hollow box with 2 mm are carried out and load/volume vs displacement curves are compared with physical compression test results in Fig. 14(b). The energy absorption of these structures is measured by numerically calculating the area under the load vs displacement curves. A numerical method, namely Trapezoidal rule [5], is used for the calculation of the area under the curve. When the domain is discretized into N equally spaced regions, the trapezoidal rule for the non-uniform grid is given by

$$\int_b^a f(x)dx \approx \frac{1}{2}\sum_{k=1}^{N}(x_{k+1} - x_k)(f(x_{k+1}) + f(x_k)) \quad (4.1)$$

where a and b are the first and last values on x coordinate (i.e $a = x_1$, $b = x_{\text{N}+1}$).

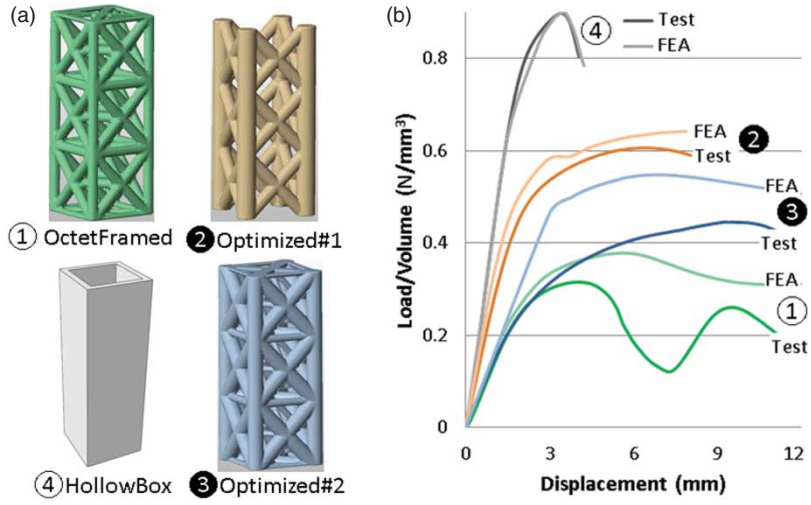

Figure 14. (a) 3D geometries of ① not optimized OctetFramed-based structure with 1.5 mm radius for each member, ❷ and ❸ optimized OctetFramed-based structures with stress-based optimization, ④ hollow box with 2 mm thickness. (b) FEA and test results of these structures in compression.

Energy absorption is calculated for the area between zero and the displacement corresponding to the maximum load/volume value from the experimental data. Since the volumes of the structures are different, a comparison of the performances of the structures can be made by dividing the energy absorption value by volume (or per weight) as shown in Tab. 4.

Table 4. Energy Absorption values of the structures tested under compression.

Structure	Energy Absorption (J)	Energy Absorption/Volume (J/mm^3)
①	9036	0.86
❷	38585	3.09
❸	50006	3.07
④	17843	2.07

The results in Fig. 14(b) show that the maximum load/volume is obtained for the hollow box structure. However, the hollow box reaches the highest load very quickly at about 3 mm (Fig. 14(b)) then plastically deformed and fails. Although the optimized structures (❷ and ❸) have lower maximum load/volume values than the hollow box, they reach their maximum load at larger displacements (at 7 mm and 9 mm, respectively) than the hollow box. Hence, the optimized structures absorb more energy per volume than the hollow box and the initial not optimized lattice structure (Tab. 1). The experimental energy absorption results show that the lattice structure optimization procedure improves the load carrying performance of the compression block and provides very efficient optimized lattice structures in terms of energy absorption under compressive loads.

5. Conclusion

In this paper, we have proposed an integrated framework for the design of lattice-based cellular structures for light weight applications. In this framework, an efficient optimization procedure has been incorporated with a novel FE modelling technique with solid elements to facilitate the non-linear analysis of cellular structures. The framework incorporates the physical experimental data with the proposed design and modeling procedure for material and performance characterization of additively manufactured lattice structures. The effectiveness of the proposed methodology has been demonstrated with the design of a compression block with periodic lattice cells to improve its load carrying performance for light weight applications. Specifically, isotropic material properties of two different materials used in two different 3D printing processes (i.e. Nylon 6 in SLS and Nylon 12 in FDM) have been predicted. The applicability of the proposed modeling technique with solid elements has also been shown to be effective by validating the non-linear simulation results with the physical compression test results. The experiments of the compression block modeled by periodic octet-based lattice cells has shown that the predicted isotropic material properties provide enough accuracy for the simulations to use for the non-linear analysis of the compression block.

OctetFramed-based unit cell has been determined to be the one that has the highest load carrying performance among various types of unit cell types based on the non-linear simulations. The load carrying performance of the lattice structures has been improved by using the proposed optimization procedure. The energy

absorption results obtained by the compression tests has proven that the proposed methodology provides improved designs that have larger energy absorption performance than the not optimized lattice structure and the hollow box. Overall, this study has illustrated that an effective design of lattice-based cellular structures for light weight applications can be achieved by considering yield and buckling failure criteria as well as the energy absorption of structures. The future work will be done for the application of the presented method for the design of real components from industry. Thus, possible applications of lattice-based cellular structures produced by additive manufacturing can be found in automotive industry.

ORCID

Recep M. Gorguluarslan http://orcid.org/[0000-0002-0550-8335]
Umesh N. Gandhi http://orcid.org/[0000-0003-1162-5279]
Raghuram Mandapati http://orcid.org/[0000-0002-8313-448X]
Seung-Kyum Choi http://orcid.org/[0000-0002-1201-7825]

References

[1] Abaqus Analysis User's Manual, "6.2.3. Eigenvalue buckling prediction", Dassault Systems, 2010.
[2] Ashby, M.F., Granta Design CES EduPack, Cambridge, 2004, http://www.grantadesign.com
[3] Bendsoe, M.; Kikuchi, N.: Generating optimal topologies in structural design using a homogenization method, Comput Methods Appl Mech Eng, 71(2), 1988, 197–224. http://dx.doi.org/10.1016/0045-7825(88)90086-2
[4] Bendsoe, M.; Sigmund, O.: Topology Optimization: Theory, Methods and Applications, Springer Verlag, New York, NY, 2003.
[5] Chapra, S.C.; Canale, R.P.: Numerical Methods for Engineers, MacGraw-Hill, NY, 2010.
[6] Deshpande, V.S.; Fleck, N.A.; Ashby, M.F.: Effective properties of the octet-truss lattice material, Journal of Mechanics and Physics of Solids, 49(8), 2001, 1747–1769. http://dx.doi.org/10.1016/S0022-5096(01)00010-2
[7] FDM Nylon 12 Data Sheet, Stratasys, http://www.stratasys.com
[8] Gibson, I., Rosen, D. W., Stucker, B.: Additive Manufacturing Technologies, Springer, New York, NY, 2010. http://dx.doi.org/10.1007/9781-4419-1120-9
[9] HyperMesh v12.0, http://www.altairhyperworks.com/Product,7,HyperMesh.aspx, Altair HyperWorks.
[10] Johnston, S.R.; Reed, M.; Wang, H.V.; Rosen, D.W.: Analysis of mesostructure unit cells comprised of octet-truss structures, in Solid Freefrom Fabrication Symposioum, 2006, Austin, TX. 421–432.
[11] Matlab Documentation Center, Optimization Toolbox, Constrained optimization, fmincon, http://www.mathworks.com/help/optim/ug/fmincon.html
[12] Netfabb Professional v5.2, http://www.netfabb.com/, netfabb GmbH 2014.
[13] Nylon 6 Data Sheet, 3Dsystems, http://www.3dsystems.com/products/datafiles/lasersintering/datasheets/DuraForm_uk.pdf
[14] Patel, J.; Choi, S.-K.: Classification approach for reliability-based topology optimization using probabilistic neural networks, Struct. Multidisc. Optim., 45, 2012, 529–543. http://dx.doi.org/10.1007/s00158-011-0711-2
[15] Rozvany, G.I.N.; Bendose M.P.; Kirsch, U.: Layout optimization of structures, Appl Mech Rev, 48, 1995, 41–119. http://dx.doi.org/10.1115/1.3005097
[16] Ruderman, A.; Choi, S.-K.; Patel, J.; Kumar, A.; Allen, J.K: Simulation-based robust design of multiscale products, Journal of Mechanical Design, 132, 2010, 101003. http://dx.doi.org/10.1115/1.4002294
[17] Seepersad, C. C.; Allen, J. K.; McDowell, D.; Mistree, F.M.: Robust Design of Cellular Materials with Topological and Dimensional Imperfections, Journal of Mechanical Design, 128(6), 2006, 1285–1297. http://dx.doi.org/10.1115/1.2338575
[18] Spadoni, A.; Ruzzene, M.; Scarpa, F.: Global and local linear buckling behavior of a chiral cellular structure, Phys. Status Solid., 242(3), 2005, 695–709. http://dx.doi.org/10.1002/pssb.200460387
[19] Thompson, S.C.; Muchnick, H.; Choi, H.-J.; McDowell, D.; Robust materials design of blast resistant panels, 11th AIAA/ISSMO Multidisciplinary Analysis and Optimization Conference, Portsmouth, VA, AIAA, 2006, 7005.
[20] Wadley, H.N.G.; Fleck, N.A.; Evans A.: Fabrication and Structural Performance of Periodic Cellular Metal Sandwich Structures, Composites Science and Technology, 63, 2003, 2331–2343. http://dx.doi.org/10.1016/S0266-3538(03)00266-5